
Learning to Delegate for Large-scale Vehicle Routing

Sirui Li*
MIT
siruil@mit.edu

Zhongxia Yan*
MIT
zxyan@mit.edu

Cathy Wu
MIT
cathywu@mit.edu

Abstract

Vehicle routing problems (VRPs) are a class of combinatorial problems with wide practical applications. While previous heuristic or learning-based works achieve decent solutions on small problem instances of up to 100 customers, their performance does not scale to large problems. This article presents a novel learning-augmented local search algorithm to solve large-scale VRP. The method iteratively improves the solution by identifying appropriate subproblems and *delegating* their improvement to a black box subsolver. At each step, we leverage spatial locality to consider only a linear number of subproblems, rather than exponential. We frame subproblem selection as a regression problem and train a Transformer on a generated training set of problem instances. We show that our method achieves state-of-the-art performance, with a speed-up of up to 15 times over strong baselines, on VRPs with sizes ranging from 500 to 3000.

1 Introduction

Vehicle routing problem (VRP) has enjoyed ample applications in logistics and ride-hailing services [21] around the world for decades. While determining the optimal solution to a VRP is NP-hard [23], there have been numerous attempts to solve VRPs both exactly and approximately: provable algorithms have been designed for specific problem instances up to size 130 [26], and powerful heuristic solvers such as LKH-3 [12] find good solutions in practice for problems of size more than 1000. However, heuristics methods often suffer from inflexibility due to extensive hand-crafting and the heavy computational burden from lengthy iterative procedures, as in the case of LKH-3. For example, LKH-3 takes more than an hour to solve a size 2000 CVRP instance (Table 1), which is impractical for applications such as real-time ride-hailing services.

More recently, machine learning methods inspired by the Pointer Network [42] provide an alternative to traditional solvers: the learning-based methods are able to greatly reduce computation time while maintaining decent solution quality on small problem instances (size less than 100), by training the network on a diverse set of problem distributions either via supervised [42] or reinforcement learning [27, 18]. However, these methods remain difficult to scale up, and only a few report results on problems of size more than 200.

Our work aims to address scalability by learning to identify smaller subproblems which can be readily solved by existing methods. Our learned subproblem selector guides the problem-solving process to focus local improvement on promising subregions. While there exists a combinatorial number of subproblems that can be selected at each step, we leverage spatial locality commonly found in

*Equal Contribution

combinatorial optimization problems to restrict the selection space dimension to be linear in the problem size. Intuitively, objects far away from each other generally have very small influence on each other’s solution and are likely to be in different tours, so they should not be part of the same subproblem. The greatly reduced search space enables us to feasibly train an attention-based model to select subproblems.

Our framework combines the best of both worlds from learning and heuristics: our network identifies promising subproblems to improve upon, dramatically speeding up the solution time. Using LKH-3 as a subsolver for the subproblems, we achieve good solution quality without the high computational burden of running LKH-3 on large problem instances. In summary, our contributions are as follows:

- We propose a learning-based framework to solve large-scale VRPs by iteratively identifying and solving small subproblems.
- We use spatial locality to restrict the subproblem selection space, allowing us to feasibly train a subproblem selector for large problem instances.
- Extensive experiments show that our method achieves the state-of-the-art result in solution quality in various distributions of VRPs while using 7x to 15x less computation time than state-of-the-art solver LKH-3 [12].

2 Preliminary: Capacitated Vehicle Routing Problems (CVRP)

In CVRP, there is a depot node 0 and city nodes $\{1, \dots, N\}$. Each city node has a demand d_i to fulfill. A vehicle with a certain capacity C starts at the depot and visits each city node i with demand d_i until the capacity C is exhausted, after which the vehicle returns to the depot to finish the route, and starts a new route from the depot again. The objective is to find a valid solution that minimizes the solution cost. Here we define the following terms:

- Route: a sequence of nodes, where the first and last node are depot 0, and the rest are city nodes. In a valid route, the sum of demands of the city nodes does not exceed C .
- Route cost: the sum of edge costs for the sequence of nodes. For an edge from node i to node j , the edge cost is the Euclidean distance between node i and j .
- Solution: a *feasible* solution consists of a set of valid routes visiting each city exactly once.
- Solution cost: the sum of route costs for all routes in the solution. An *optimal* solution is a feasible solution with the minimum solution cost.
- Subproblem: the depot node, a subset of city nodes, and corresponding demands.

3 Related Work

Classical methods. Heuristics for solving combinatorial optimization problems have been studied for decades. The most powerful methods, such as local search [1], genetic algorithms [32], and ant colony methods [9], involve iteratively improving the solution in a hand-designed neighborhood. For example, move, swap [44], and 2-opt [8] are well-known heuristics for the traveling salesman and vehicle routing problems. The state-of-the-art VRP solver LKH-3 [12] uses the Lin–Kernighan heuristic [24] as a backbone, which involves swapping pairs of sub-tours to create new tours.

For large problems, sophisticated *meta-heuristics* layer on top of low level heuristics, including Tabu Search with Adaptive Memory [36], guided local search [43], and Large Neighborhood Search [31]. The inspiration for our work derives from Partial OPTimization Metaheuristic Under Special Intensification Conditions (POPMUSIC), which iteratively optimizes on problem subparts, and has been used to solve problems as diverse as map labeling [22], berth allocation [20], and p -median clustering [35]. Despite the promise of the POPMUSIC framework for large-scale combinatorial optimization, the impact of certain design choices is not well understood, such as the subproblem selection ordering and size [38]. For example, it is not clear how to meaningfully order the subproblems. One early work in this direction demonstrated that a last-in-first-out stack order performs better than random [3]. Our work provides a natural approach to order the subproblems based on expected improvement.

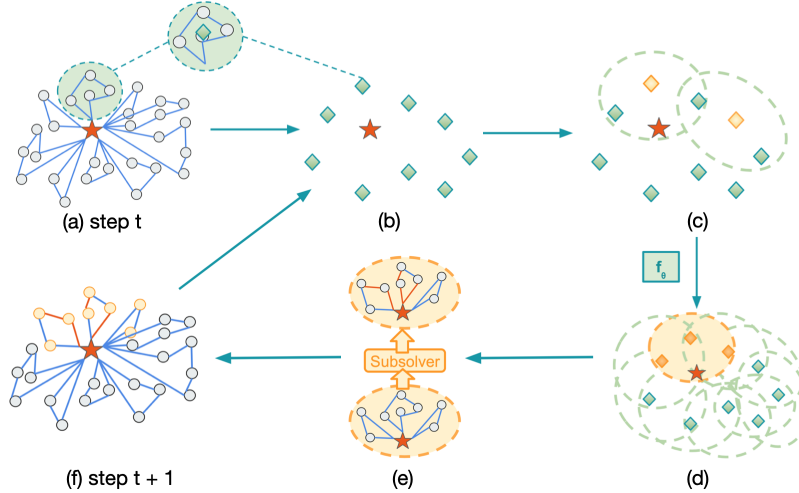


Figure 1: **Our iterative framework for VRP.** (a) At each time step, we start with a current solution X . Circles are city nodes, blue lines are routes, and the red star is the depot. (b) We aggregate each route by taking the centroid of all city nodes in the route. (c) For each route, we define a corresponding subproblem as the k -nearest neighbors of the route. Two such subproblems with $k = 3$ are shown. (d) Our subproblem selector selects a subproblem S (yellow). (e) We feed S into the subsolver to get a new subsolution X'_S . The red edges are updated by the subsolver. (f) We update X to new solution X' with X'_S , then repeat (b)-(f).

Deep learning methods. Recently, there has been a surge of interest in training deep neural networks (DNN) to solve combinatorial problems. As observed by Kwon et al. [19], most methods fall into one of the following two categories: 1) *construction methods* [27, 18], where an autoregressive model such as the Pointer Network [42] directly outputs a solution, and 2) *improvement methods* [6, 13], where the DNN iteratively performs local updates to the solution, resembling local search.

These methods are approaching the solution quality of LKH-3 [12] on small problem instances. For example, Kwon et al. [19] extends a constructive approach [18] to encourage more diverse output samples on $N \leq 100$ VRPs. Among improvement methods, Lu et al. [25] learn a meta-controller to select among a set of local search heuristics, marking the first learning-based approach to outperform LKH-3 on $N \leq 100$ VRPs. Despite these successes, learning-based approaches for large-scale VRPs are poorly understood. In particular, all of the aforementioned methods are trained using deep reinforcement learning; for large problems, trajectory collection becomes prohibitively expensive.

Scaling up learning methods. A few early works have just begun to investigate scaling of learned networks for NP-hard graph problems. For example, Ahn et al. [2] propose an effective iterative scheme called *learning-what-to-defer* for maximum independent set. At each stage, and for each node in the graph, the network either outputs the solution for the node, or defers the determination to later stages. Song et al. [34] proposes an imitation-learning-based pipeline for Integer Linear Programs (ILP), where at each stage they partition all variables into disjoint subsets, and use the Gurobi [11] ILP solver to solve the partitions. Due to differences in graph structure, our work presents a more natural scheme to handle VRP constraints and structures.

4 An Iterative Framework for CVRPs

While CVRPs are NP-hard and thus require worst-case exponential time in the problem size to solve optimally, typical CVRPs exhibit structure that practical solvers may exploit. We hypothesize that in such situations, the larger problem can be efficiently approximately solved as a sequence of smaller subproblems, which can be *delegated* to efficient subsolvers. To test this hypothesis, we propose a learning-based, iterative framework with two components: 1) a *subsolver* capable of solving a small problem instance (exactly or approximately), and 2) a *learned model* for identifying suitable subproblems within a larger problem to delegate to the subsolver.

Algorithm 1: Learning to Delegate

Input: Problem instance P , initialized solution X , subproblem selector f_θ , subsolver Subsolver , number of steps T , parameter k denoting the size of subproblems

```
1 for Step  $t = 1: T$  do  
2    $\mathcal{S}_{k,\text{local}} \leftarrow \text{ConstructSubproblems}(P, X, k)$   
3    $S \leftarrow f_\theta(\mathcal{S}_{k,\text{local}})$   
4    $X'_S \leftarrow \text{Subsolver}(S)$   
5    $X \leftarrow X'_S \cup X_{P \setminus S}$   
6 end for
```

We illustrate our iterative framework in Figure 1, which takes in a problem instance P with a feasible initial solution X_0 . At each step, given the current solution X , we select a smaller subproblem $S \subset P$ with our learned model f_θ then apply the subsolver to solve S ; we then update X with the new solution for S . To maintain feasibility after an update, we restrict S to be the set \mathcal{S} of visited cities of a *subset of routes* from X . Since routes with cities in $P \setminus S$ remain valid routes, we obtain a new feasible solution $X' = X'_S \cup X_{P \setminus S}$, where X'_S is the subsolution for S and $X_{P \setminus S}$ consists of unselected routes from X . Intuitively, a strong f_θ should identify a subproblem S such that the subsolver solution X'_S results in a large improvement in objective from X to X' .

4.1 The Restricted Subproblem Selection Space

As the number of routes in P is $R = O(N)$, the cardinality of the selection space \mathcal{S} is $O(2^R)$, which is exponential in the problem size N and difficult for learned models to consider. If we restrict each subproblem to cities from exactly k routes, there are still $\binom{R}{k} = O(R^k)$ subproblems to consider. Therefore we further restrict selection to subproblems with spatial locality. As shown in Figure 1(d), we only consider subproblems from $\mathcal{S}_{k,\text{local}}$, where each subproblem is centered around a particular route r and contains the k routes whose centroids have the smallest Euclidean distance to the centroid of r . In this way, we reduce the selection space to $|\mathcal{S}_{k,\text{local}}| = R = O(N)$ from $|\mathcal{S}| = O(2^N)$. In Algorithm 1, we refer to this restriction as `ConstructSubproblems`. Our restriction to a local selection space is motivated by the fact that many combinatorial optimizations problems have inherent spatial locality, i.e. problem entities are more strongly affected by nearby entities than faraway entities. Earlier heuristical methods such as POPMUSIC [37] leverage similar spatial locality.

5 Learning to Delegate

In this section, we discuss criteria for selecting subproblems, and how to train the subproblem selector.

Improvement as the criteria for subproblem selection. Given a selected subproblem S with a current solution X_S on the subproblem, we obtain from LKH-3 a new solution X'_S on the same subproblem (step (d) to (e) in Figure 1). We then define the *immediate improvement*

$$\delta(S) = c(X_S) - c(X'_S) \quad (1)$$

where $c(X)$ is the total cost of the solution X and $\delta(S)$ is the improvement in the solution cost. In this way, the sum of improvements along T steps is the total improvement in solution quality. As we empirically find that providing the previous subsolution X_S to the subsolver may trap the subsolver in a local optimum, we withhold X_S from the solver and thus may see non-positive improvement $\delta(S) \leq 0$, especially after many steps of subproblem selection. At test time, to avoid worsening the objective, we adopt a hill-climbing procedure such that when $\delta(S) \leq 0$, we keep X_S instead of X'_S (Figure 1, step (e)). We do not select the same non-improving subproblem S again with proper masking. The hill-climbing and masking procedures are applied to both our subproblem-selection network f_θ and the three heuristic selection rules, described in 6.1, to maintain a fair comparison.

Subproblem selection. The goal of our subproblem selector is to select the subproblem leading to the best *immediate* improvement. While our subproblem selection does not directly optimize for the total improvement, we observe that (1) our subsolver may perform many low-level operations internally, so high-level problem selection may still benefit greatly from maximizing the immediate

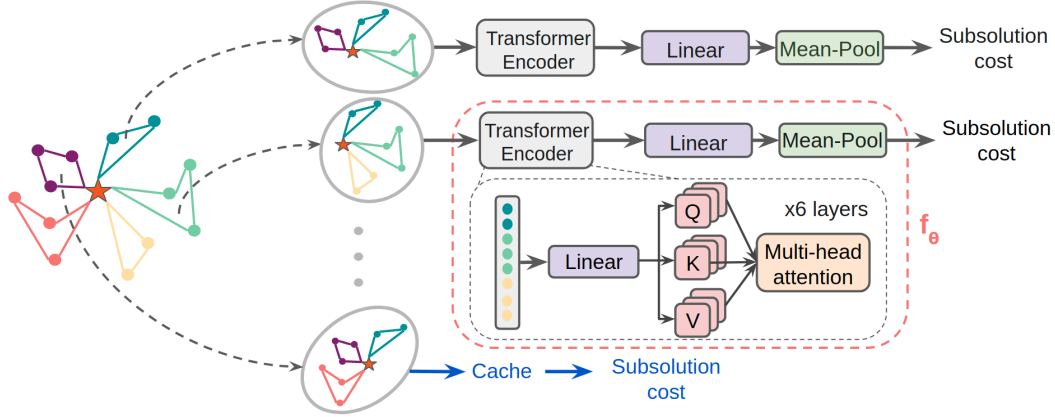


Figure 2: **Our transformer architecture.** At each step of our framework (Figure 1(c)), we featurize subproblem $S \in \mathcal{S}_{k,\text{local}}$ into a column vector of unordered cities. We apply the Transformer encoder with multiple multi-head attention layers and a final linear layer, before mean-pooling over the cities to generate the predictions $f_\theta(S)$, which we fit to the subsolution cost $c(X'_S)$. When possible, we retrieve a previously predicted subproblem from a cache to minimize computation.

improvement, and (2) numerous reinforcement learning approaches to VRP [45, 16] choose a small discount factor such as $\gamma = 0.25$ when optimizing a multi-step objective $\sum_{t=1}^T \gamma^t \delta_t$, as doing so encourage faster convergence. Moreover, our subproblem selector may instead be trained on multi-step search data to select subproblems offering the best multi-step improvement.

Ground-truth labels Our restricted selection space allows us to enumerate all possible subproblems at each step. In a typical large scale CVRP instance with $N = 2000$ cities, a solution consists of roughly $R = 200$ routes, so the size of the selection space is 200. We obtain the immediate improvement $\delta(S)$ by running the subsolver on each subproblem $S \in \mathcal{S}_{k,\text{local}}$. Although our enumeration strategy is feasible for generating training data, it is much too slow to execute on a test CVRP instance. However, if our subproblem selector can predict the best immediate improvement at test time (that is, without running the subsolver on multiple subproblems), then we can combine the best of both worlds to obtain a fast and accurate selection strategy.

Selection strategies: regression vs classification Given a labeled dataset, we may learn a model to perform either regression or classification to identify the best subproblem. In the context of imitation learning with a greedy expert, the former learns a *value function* while the latter learns a *policy*. Due to space limitation, we focus discussion on regression and reserve the comparison with classification for Appendix A.1. The regression-based subproblem selector trains a regression model f_θ to predict the subsolution cost $c(X'_S)$, from which we simply compute $\arg \max_S c(X'_S) - f_\theta(S)$ to select the best subproblem.

Network architecture. We define f_θ based on the Transformer encoder architecture [40]. The input for each subproblem S is the unordered set of featurized cities in S . The features for each city consist of the demand d and the location of the city (x, y) relative to the depot. As we do not feed the existing subsolution X_S to the subsolver, the dense multi-head attention mechanism does not need to be modified to take the routes in X_S into account. The output of the Transformer encoder is fed into a linear layer then mean-pooled to obtain the scalar prediction $f_\theta(S)$.

Loss function. We define our loss function to be the Huber loss [14], which we empirically found to be more stable than mean squared error,

$$L(\theta; S) = \begin{cases} \frac{1}{2}(f_\theta(S) - c(X'_S))^2, & \text{if } |f_\theta(S) - c(X'_S)| \leq 1 \\ |f_\theta(S) - c(X'_S)| - \frac{1}{2}, & \text{otherwise} \end{cases} \quad (2)$$

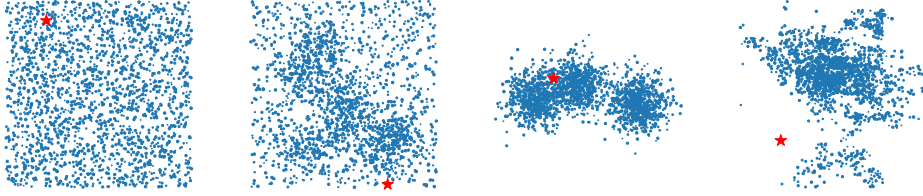


Figure 3: **Instances from $N = 2000$ CVRP distributions.** From left to right: instance from uniform, mixed ($n_c = 7$ cluster centers), clustered ($n_c = 3$ cluster centers), and real-world. The red star is the location of the depot, while blue dots are cities sized proportional to demand.

6 Experiments and Analysis

We illustrate the CVRP distributions considered in our work in Figure 3. We perform extensive experiments to evaluate our learning framework. We aim to answer the following questions:

1. **Uniform distribution.** How does our method compare with baselines on the uniform data distribution, in terms of solution time and quality?
2. **Clustered distributions.** How does our method perform on clusters of cities?
3. **Generalization.** Can our model generalize, such as to larger or real-world instances?
4. **Other VRP variants.** Can the method address more sophisticated VRPs, e.g., CVRP with Time Windows (CVRPTW) [33], VRP with Mixed Pickup and Delivery (VRPMPD) [30]?

Due to space limitation, we reserve additional ablation on the choice of subproblem size (parameterized by k) and additional analysis of asymptotic behavior for Appendix A.6.

6.1 Setup

Due to space limitation, we briefly describe experimental setup in the main text and defer full details to Appendix A.2. Given a particular distribution of VRP, we generate separate sets of training, validation, and test problem instances. Unless otherwise stated, our validation and test sets contain 40 instances each. For each problem instance, we generate a rough initial solution by partitioning it into disjoint subsets of cities and briefly running the subsolver on each subset. Due to its generality, we use LKH-3 [12] as the subsolver for all VRP distributions.

We generate the training set by running our iterative framework and selecting subproblems by enumerating the subsolver on all $S \in \mathcal{S}_{k,\text{local}}$. As many subproblems remain unchanged from X to X' , we use previously cached subsolutions when possible instead of re-running the subsolver. While generation times differ depending on several factors, typically it takes less than ten hours with 200 Intel Xeon Platinum 8260 CPUs to generate a training set of 2000 instances.

To avoid training multiple models for different problem sizes N , we train a single model for each VRP distribution with combined data from $N \in \{500, 1000, 2000\}$. Training takes at most 8 hours on a single NVIDIA V100 GPU. To exploit symmetry in problem instances, we apply rotation and flip augmentation at training time. To evaluate trained selectors on a problem instance, we run the iterative selection framework on a single CPU, with disabled multithreading and no GPU.

We select the best hyperparameters via manual search based on validation set performance. We record final results on the test set as the mean and standard error over 5 runs with different random seeds.

Baselines. Consistent with our choice of subsolver, a key baseline from the literature is **LKH-3** [12]. We run the LKH-3 solver on the full problem instance for 30000 local update steps, which takes 2-3 hours on average for $N = 2000$. For fairness, we warm-start LKH-3 with our initialization. We also compare against OR Tools [28], another open source solver. We set 15 min as the time-out for OR Tools, which converges in all settings.

To compare against previous learning methods, we include AM [18] and NeuRewriter [6]. Most of the previous work do not outperform LKH-3 even on small problem sizes, and learning methods

Table 1: **Performance and computation time for Uniform CVRP.** For problem instance sizes $N \in \{500, 1000, 2000\}$, we report the objective values (*lower* is better) of our method and baseline methods, averaged across all instances in the test set. Note that the cost is the total distance of routes in the solution. LKH-3 (30k) runs LKH-3 for 30k steps to near convergence, while LKH-3 (95%) runs LKH-3 until 95% of the total improvement has been attained. Random, Count-based, Max Min Distance, and Ours (Short) run until matching LKH-3 (95%) in solution quality with the speedup reported in parentheses, while Ours (long) runs for twice amount time as Ours (Short).

Method	N = 500		N = 1000		N = 2000	
	Cost	Time	Cost	Time	Cost	Time
LKH-3 (95%)	62.00	4.4min	120.02	18min	234.89	52min
LKH-3 (30k)	61.87	30min	119.88	77min	234.65	149min
OR Tools	65.59	15min	126.52	15min	244.65	15min
AM sampling	69.08	4.70s	151.01	17.40s	356.69	32.29s
AM greedy	68.58	25ms	142.84	56ms	307.86	147ms
NeuRewriter	73.60	58s	136.29	2.3min	257.61	8.1min
Random	61.99	71s (3.8x)	120.02	3.2min (5.5x)	234.88	6.4min (8.0x)
Count-based	61.99	59s (4.5x)	120.02	2.1min (8.2x)	234.88	5.3min (10x)
Max Min	61.99	59s (4.5x)	120.02	2.5min (7.0x)	234.89	5.2min (10x)
Ours (Short)	61.99	38s (7.0x)	119.87	1.5min (12x)	234.89	3.4min (15x)
Ours (Long)	61.70	76s	119.55	3.0min	233.86	6.8min

have had more difficulty generalizing to larger instances. In fact, all of the previous methods are trained on problems of size $N \leq 100$, and we have found that they generally do not yield good outcomes on $N \geq 500$, without modifying the architecture and doing extensive retraining. The AM and NeuRewriter results demonstrate the difficulty of scaling up previous learning methods. We do not warm-start OR-Tools, AM, and NeuRewriter because we find empirically that these methods have limited solution capability, and they do not improve from our decent warm-start.

To validate our subproblem selector’s ability to learn a meaningful subproblem-selection order, we design three additional baselines that employ our iterative framework using *hand-crafted heuristics* to select subproblems. The three heuristics that we use are: (1) Random, selecting subproblem S from $\mathcal{S}_{k,\text{local}}$ uniformly; (2) Count-based, which avoids repetitive selections by selecting the subproblem centered at the route whose city nodes have been selected cumulatively the least often in previous steps; and (3) Max Min Distance, which encourages coverage of the entire problem instance by selecting subproblems with the maximum distance from the nearest centroid of previously selected subproblems. We run the heuristic baselines with the same setup as our subproblem selector.

Metrics. We refer to two metrics to compare our method against baseline methods.

1. **Improvement over method X:** at a specified computation time, the improvement of method Y over method X is the total improvement of method Y minus that of method X.
2. **Speedup over method X:** at a specified solution quality that method X attains, the speedup of method Y over method X is the computation time required for method X to attain the solution quality divided by that for method Y to attain the solution quality.

We often report the numerical speedup over LKH-3 at 95% solution quality (i.e. 95% of the maximum improvement attained by LKH-3) as LKH-3 takes an exorbitant amount of time to attain the last 5% of improvement; reporting the speedup at 100% LKH-3 solution quality would inflate the speedup.

6.2 Uniform CVRP Distribution

As seen in Table 1, our method achieves the best performance for all problem sizes, matching LKH-3’s solution quality with more than 7x to 15x less computation time and offering even more improvements with longer computation time. Although we need to evaluate all $R = O(N)$ subproblems of the initial solution in the first step with our subproblem selector, the subsequent per-step computation time of our method after the first step is mostly independent of the problem size N since we only need to evaluate subproblems that have changed.

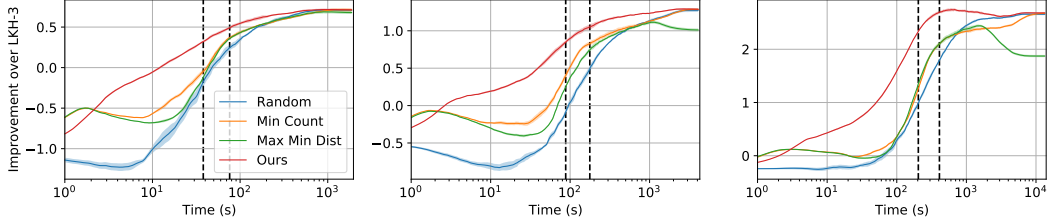


Figure 4: **Improvement over LKH-3 for Uniform CVRP.** The x-axis is the computation time of our method and LKH-3 and extends until LKH-3 has completed 30k steps. The dotted vertical lines represent the computation times of Ours (Short) and Ours (Long) from Table 1. The three subplots correspond to $N = 500$ (left), $N = 1000$ (middle), and $N = 2000$ (right).

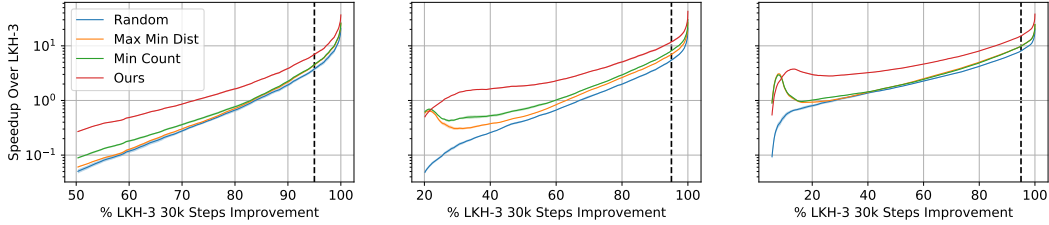


Figure 5: **Speedup over LKH-3 for Uniform CVRP.** The x-axis is the solution quality attained, measured as a percentage of the LKH-3’s maximum improvement. The dotted vertical line represents the 95% solution quality which we use to compute the numerical speedup, as mentioned in Table 1. The three subplots correspond to $N = 500$ (left), $N = 1000$ (middle), and $N = 2000$ (right).

Running LKH-3 for 30k local update steps achieves superior performance to all previous other heuristic and learning-based baselines. Its solution quality scales well to large problem sizes, yet the solution time is significantly longer. Previous learning-based methods, although fast, result in much worse solution qualities. Our heuristic baselines Random, Count-based, and Max Min Distance demonstrate that our iterative framework, even without the learned subproblem selector, may achieve over 5x to 10x speedup over LKH-3. Nevertheless, our results demonstrate that learning the subproblem selector may offer an additional 1.5x speedup over non-learning heuristics.

In Figure 4, we demonstrate the solution quality of our method and baselines compared to LKH-3. We see that, compared to baseline methods, the learned subproblem selector begets the best solution quality when run for a reasonable amount of time. The improvement of most methods based on our iterative framework converge when run for an exorbitant amount of time; this is unsurprising, as Random and other baselines are eventually able to select all subproblems offering improvements.

In Figure 5, we demonstrate the speedup of our method over LKH-3, comparing to baseline methods. The speedup is often significant even at low levels of solution quality, and improves with higher solution quality. The speedup is not as meaningful past 95% of LKH-3’s maximum improvement, as LKH-3 takes an exorbitant amount of time to attain the last 5% of improvement.

6.3 Clustered and Mixed CVRP Distributions

We further examine the framework’s performance on CVRP distributions with clusters, such as studied in [7, 39]. We generate a clustered instance by first sampling (x, y) locations of n_c cluster centroids then sampling the cities around the centroids. The mixed distribution samples 50% of the cities from a uniform distribution and the rest from around cluster centers. We generate a dataset of clustered and mixed instances for $(N, n_c) \in$

Table 2: **Speedup for $N = 2000$ Clustered and Mixed CVRPs at 95% maximum LKH-3 solution quality.**

Setting		$n_c = 3$	$n_c = 5$	$n_c = 7$
Clustered	Ours	26x	18x	25x
	Random	11x	7.5x	9.0x
Mixed	Ours	13x	14x	14x
	Random	6.6x	6.4x	7.6x

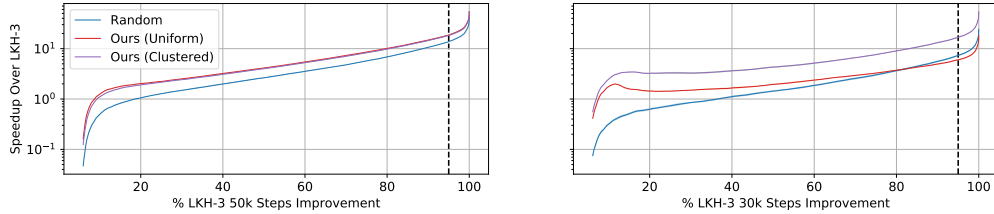


Figure 6: **Speedup in Out-of-distribution CVRPs.** We report the speedup when evaluating our model without finetuning on the $N = 3000$ uniform distribution (left) and $N = 2000$ real-world distribution (right). Ours (Uniform) and Ours (Clustered) are trained on the uniform and clustered CVRP distributions, respectively. Note that LKH-3 is run for 50k steps for the $N = 3000$ instance.

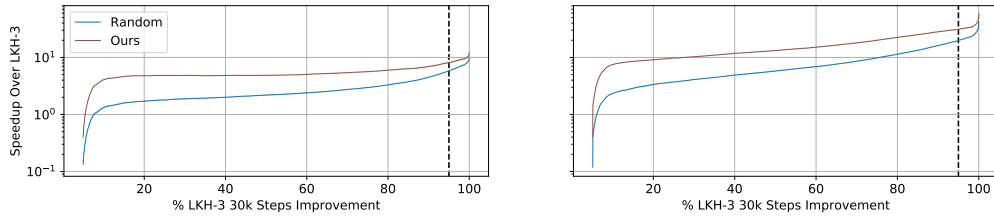


Figure 7: **Speedup in other $N = 2000$ VRP Variants.** We report the speedup when evaluating our method on CVRPTW (left) and VRPMPD (right).

$\{500, 1000, 2000\} \times \{3, 5, 7\}$ and train a single model on the entire dataset. Due to space limitation, we provide more details about the data distribution and full results in the Appendix A.3.

Table 2 reports the speedup of our learned subproblem selector and the Random baseline over LKH-3 at the 95% maximum LKH-3 solution quality. We can see that our method offers at least a 2x speedup over the Random baseline in all settings. Interestingly, we see a larger speedup over LKH-3 for the clustered distribution than that for the mixed distribution and uniform distribution in Table 1.

6.4 Generalization

We study how our subproblem selector generalize to a uniform CVRP distribution with larger problem size $N = 3000$ and to a real-world CVRP distributions, both of which are unseen at training time. The real world CVRP distribution derives from a CVRP dataset [4] consisting of 10 very-large-scale instances on 5 Belgium regions with N ranging from 3000 to 30000 and randomly generated demand distribution. To generate an instance, we subsample the cities in a region without replacement to a smaller size $N = 2000$, while regenerating the demand to have the same distribution as our uniform and cluster training dataset. The original and subsampled dataset are visualized in Appendix A.4.

We apply subproblem selectors trained on uniform and clustered data without finetuning on the new data distributions and report the speedup comparison with the Random baseline in Figure 6. We see that when transferring to $N = 3000$, the subproblem selectors trained on uniform and clustered data offer similar performance. However, the model trained on the clustered distribution generalizes well to the real-world distribution while the model trained on the uniform distribution fails to generalize, with worse speedup than the Random baseline. These results suggest that the domain variability of the clustered distribution strongly improves generalization performance.

6.5 Other VRP Variants

While our previous experiments focus on varying the distribution of city locations in CVRP, here we consider two VRP variants with uniform city distribution but with additional constraints: CVRPTW [33] and VRPMPD [30]. The former specifies a hard time window constraint for visiting each city, while the latter specifies pick up and delivery constraints in addition to capacity constraint. A detailed description of the variants can be found in Appendix A.5.

Similar to the CVRP distributions, we observe a significant speedup from applying our iterative framework, with additional speedup when using a learned subproblem selector. For CVRPTW, our method offers a 8.2x speedup while our Random baseline offers a 5.9x speedup; for VRPMPD, our method offers a 31x speedup while our Random baseline offers a 20x speedup. We suspect that the time window constraint in CVRPTW is more difficult to learn for the subproblem selector, as it imposes strict orderings on the order of city visitations.

7 Conclusion

This paper presents a learning-based framework for large VRPs, which learns which subproblems to delegate to a subsolver. Spatial locality in VRPs allows us to learn the subproblem selector over a reduced subproblem space. The proposed method outperforms the state-of-the-art VRP solver LKH-3 on problems of sizes up to 3000, with an order of magnitude less computation time. As future work, we plan to apply our method to other combinatorial optimization problems with spatial locality. We believe that our learning framework can serve as a powerful technique for both the learning and operations research communities to scale up combinatorial optimization solvers.

Negative Social Impact. Enabling more efficient solutions of large-scale VRPs may exhibit negative externalities such as inducing additional traffic from delivery vehicles and centralizing services that pose a stronger competition to brick-and-mortar retail.

References

- [1] Aarts, E., Aarts, E. H., and Lenstra, J. K. (2003). *Local search in combinatorial optimization*. Princeton University Press.
- [2] Ahn, S., Seo, Y., and Shin, J. (2020). Learning what to defer for maximum independent sets. In *International Conference on Machine Learning*, pages 134–144. PMLR.
- [3] Alvim, A. C. and Taillard, E. D. (2013). Popmusic for the world location-routing problem. *EURO Journal on Transportation and Logistics*, 2(3):231–254.
- [4] Arnold, F., Gendreau, M., and Sörensen, K. (2019). Efficiently solving very large-scale routing problems. *Computers & Operations Research*, 107:32–42.
- [5] Błażewicz, J., Domschke, W., and Pesch, E. (1996). The job shop scheduling problem: Conventional and new solution techniques. *European journal of operational research*, 93(1):1–33.
- [6] Chen, X. and Tian, Y. (2019). Learning to perform local rewriting for combinatorial optimization. In Wallach, H., Larochelle, H., Beygelzimer, A., d’Alché-Buc, F., Fox, E., and Garnett, R., editors, *Advances in Neural Information Processing Systems*, volume 32. Curran Associates, Inc.
- [7] Christofides, N., Mingozzi, A., and Toth, P. (1979). Loading problems. N. Christofides and al., editors, *Combinatorial Optimization*, pages 339–369.
- [8] Croes, G. A. (1958). A method for solving traveling-salesman problems. *Operations research*, 6(6):791–812.
- [9] Dorigo, M., Birattari, M., and Stutzle, T. (2006). Ant colony optimization. *IEEE computational intelligence magazine*, 1(4):28–39.
- [10] Gehring, H. and Homberger, J. (1999). A parallel hybrid evolutionary metaheuristic for the vehicle routing problem with time windows. In *Proceedings of EUROGEN99*, volume 2, pages 57–64. Citeseer.
- [11] Gurobi Optimization, L. (2021). Gurobi optimizer reference manual.
- [12] Helsgaun, K. (2017). An extension of the lin-kernighan-helsgaun tsp solver for constrained traveling salesman and vehicle routing problems. <http://akira.ruc.dk/~keld/research/LKH-3/>.
- [13] Hottung, A. and Tierney, K. (2020). Neural large neighborhood search for the capacitated vehicle routing problem. In *24th European Conference on Artificial Intelligence (ECAI 2020)*.
- [14] Huber, P. J. (1992). Robust estimation of a location parameter. In *Breakthroughs in statistics*, pages 492–518. Springer.
- [15] Kallehauge, B., Larsen, J., Madsen, O. B., and Solomon, M. M. (2005). Vehicle routing problem with time windows. In *Column generation*, pages 67–98. Springer.
- [16] Khalil, E. B., Dai, H., Zhang, Y., Dilkina, B., and Song, L. (2017). Learning combinatorial optimization algorithms over graphs. In *Advances in Neural Information Processing Systems*.
- [17] Kohl, N., Desrosiers, J., Madsen, O. B., Solomon, M. M., and Soumis, F. (1999). 2-path cuts for the vehicle routing problem with time windows. *Transportation Science*, 33(1):101–116.
- [18] Kool, W., van Hoof, H., and Welling, M. (2019). Attention, learn to solve routing problems! In *International Conference on Learning Representations*.
- [19] Kwon, Y.-D., Choo, J., Kim, B., Yoon, I., Gwon, Y., and Min, S. (2020). Pomo: Policy optimization with multiple optima for reinforcement learning. In Larochelle, H., Ranzato, M., Hadsell, R., Balcan, M. F., and Lin, H., editors, *Advances in Neural Information Processing Systems*, volume 33, pages 21188–21198. Curran Associates, Inc.
- [20] Lalla-Ruiz, E. and Voss, S. (2016). Popmusic as a matheuristic for the berth allocation problem. *Annals of Mathematics and Artificial Intelligence*, 76(1-2):173–189.

- [21] Laporte, G. (2009). Fifty years of vehicle routing. *Transportation science*, 43(4):408–416.
- [22] Laurent, M., Taillard, É. D., Ertz, O., Grin, F., Rappo, D., and Roh, S. (2009). From point feature label placement to map labelling. In *Proceedings, metaheuristic international conference (MIC'09), Hamburg*. Citeseer.
- [23] Lenstra, J. K. and Kan, A. R. (1981). Complexity of vehicle routing and scheduling problems. *Networks*, 11(2):221–227.
- [24] Lin, S. and Kernighan, B. W. (1973). An effective heuristic algorithm for the traveling-salesman problem. *Operations research*, 21(2):498–516.
- [25] Lu, H., Zhang, X., and Yang, S. (2020). A learning-based iterative method for solving vehicle routing problems. In *International Conference on Learning Representations*.
- [26] Lysgaard, J., Letchford, A. N., and Eglese, R. W. (2004). A new branch-and-cut algorithm for the capacitated vehicle routing problem. *Mathematical Programming*, 100(2):423–445.
- [27] Nazari, M., Oroojlooy, A., Snyder, L., and Takac, M. (2018). Reinforcement learning for solving the vehicle routing problem. In Bengio, S., Wallach, H., Larochelle, H., Grauman, K., Cesa-Bianchi, N., and Garnett, R., editors, *Advances in Neural Information Processing Systems*, volume 31. Curran Associates, Inc.
- [28] Perron, L. and Furnon, V. (2019). Or-tools.
- [29] Renaud, J. and Boctor, F. F. (2002). A sweep-based algorithm for the fleet size and mix vehicle routing problem. *European Journal of Operational Research*, 140(3):618–628.
- [30] Salhi, S. and Nagy, G. (1999). A cluster insertion heuristic for single and multiple depot vehicle routing problems with backhauling. *Journal of the operational Research Society*, 50(10):1034–1042.
- [31] Shaw, P. (1998). Using constraint programming and local search methods to solve vehicle routing problems. In *International conference on principles and practice of constraint programming*, pages 417–431. Springer.
- [32] Sivanandam, S. and Deepa, S. (2008). Genetic algorithms. In *Introduction to genetic algorithms*, pages 15–37. Springer.
- [33] Solomon, M. M. (1987). Algorithms for the vehicle routing and scheduling problems with time window constraints. *Operations research*, 35(2):254–265.
- [34] Song, J., Lanka, R., Yue, Y., and Dilkina, B. (2020). A general large neighborhood search framework for solving integer linear programs. In Larochelle, H., Ranzato, M., Hadsell, R., Balcan, M. F., and Lin, H., editors, *Advances in Neural Information Processing Systems*, volume 33, pages 20012–20023. Curran Associates, Inc.
- [35] Taillard, É. D. (2003). Heuristic methods for large centroid clustering problems. *Journal of heuristics*, 9(1):51–73.
- [36] Taillard, É. D., Gambardella, L. M., Gendreau, M., and Potvin, J.-Y. (2001). Adaptive memory programming: A unified view of metaheuristics. *European Journal of Operational Research*, 135(1):1–16.
- [37] Taillard, É. D. and Voss, S. (2002). Popmusic—partial optimization metaheuristic under special intensification conditions. In *Essays and surveys in metaheuristics*, pages 613–629. Springer.
- [38] Taillard, É. D. and Voß, S. (2018). *POPMUSIC*, pages 687–701. Springer International Publishing, Cham.
- [39] Uchoa, E., Pecin, D., Pessoa, A., Poggi, M., Vidal, T., and Subramanian, A. (2017). New benchmark instances for the capacitated vehicle routing problem. *European Journal of Operational Research*, 257(3):845–858.

- [40] Vaswani, A., Shazeer, N., Parmar, N., Uszkoreit, J., Jones, L., Gomez, A. N., Kaiser, L. u., and Polosukhin, I. (2017). Attention is all you need. In Guyon, I., Luxburg, U. V., Bengio, S., Wallach, H., Fergus, R., Vishwanathan, S., and Garnett, R., editors, *Advances in Neural Information Processing Systems*, volume 30. Curran Associates, Inc.
- [41] Veličković, P., Cucurull, G., Casanova, A., Romero, A., Liò, P., and Bengio, Y. (2018). Graph Attention Networks. *International Conference on Learning Representations*.
- [42] Vinyals, O., Fortunato, M., and Jaitly, N. (2015). Pointer networks. In Cortes, C., Lawrence, N., Lee, D., Sugiyama, M., and Garnett, R., editors, *Advances in Neural Information Processing Systems*, volume 28. Curran Associates, Inc.
- [43] Voudouris, C. and Tsang, E. P. (2003). Guided local search. In *Handbook of metaheuristics*, pages 185–218. Springer.
- [44] Wu, C., Shankari, K., Kamar, E., Katz, R., Culler, D., Papadimitriou, C., Horvitz, E., and Bayen, A. (2016). Optimizing the diamond lane: A more tractable carpool problem and algorithms. In *2016 IEEE 19th International Conference on Intelligent Transportation Systems (ITSC)*, pages 1389–1396. IEEE.
- [45] Yolcu, E. and Póczos, B. (2019). Learning local search heuristics for boolean satisfiability. In Wallach, H., Larochelle, H., Beygelzimer, A., d'Alché-Buc, F., Fox, E., and Garnett, R., editors, *Advances in Neural Information Processing Systems*, volume 32. Curran Associates, Inc.

A Appendix

Contents

A.1	Regression vs Classification for Subproblem Selection	14
A.2	Experiment Setup	16
A.3	Clustered and Mixed CVRP	18
A.4	Out-of-distribution CVRPs	22
A.4.1	Uniform CVRP with $N = 3000$	22
A.4.2	Real-world CVRP	22
A.5	VRP Variants	24
A.5.1	CVRPTW (Capacitated Vehicle Routing Problem with Time Windows)	24
A.5.2	VRPMPD (Vehicle Routing Problem with Mixed Pickup and Delivery)	24
A.6	Ablation Studies	26
A.6.1	Subproblem Size k and Asymptotic Behavior in Uniform CVRP	26
A.6.2	Subproblem Regression vs Classification	26

A.1 Regression vs Classification for Subproblem Selection

While we focus on regression in the main text, we discuss how to frame subproblem selection as classification here, and compare results and discuss tradeoffs with regression-based subproblem selection in Appendix A.6.

Subproblem selection as classification. The goal of a classification-based subproblem selector is to select the subproblem which results in the best immediate improvement when solved by the subsolver.

Label transformation. Optimally, we would like our subproblem selector to select the subproblem with the best immediate improvement. However, since we want to avoid overpenalizing the subproblem selector for putting probability mass on a slightly suboptimal selection, we construct a softmax soft label based on $\delta(S)$ with temperature parameter τ rather than a one-hot hard label, which corresponds to $\tau \rightarrow 0$

$$\ell(S) = \frac{e^{\delta(S)/\tau}}{\sum_{S' \in \mathcal{S}_{k,\text{local}}} e^{\delta(S')/\tau}} \quad (3)$$

Network Architecture. An important consequence of subproblem classification is that all subproblems must be considered jointly. This requires a different architecture than presented in Section 5. Intuitively, in order to consider which subproblem is *best*, the other subproblems must be taken into account. In the regression context, a local measure of improvement is all that is needed. More precisely, as subproblem classification inherently requires feed-forward and back-propagation computation over all subproblems $S \in \mathcal{S}_{k,\text{local}}$ for a single problem P , our choice of architecture must address this constraint to feasibly train with a large enough batch of problems. Unlike in subproblem regression, we cannot simply sample batches of subproblems from the set of all problem instances to fit individually; each computation in classification entails a softmax over $|\mathcal{S}_{k,\text{local}}|$ subproblems from the same problem instance. Therefore, our classification-based subproblem selector consists of a graphical attention network (GAT) backbone [41], which shares computation and memory between overlapping subproblems in the same problem instance, permitting the use of large batches of problem instances P to increase training stability.

We illustrate the nodes and edges of the graph attention in Figure 8. Given a problem instance P , we define three types of graph nodes: one *city-node* per city in P , one *route-node* per route r in the current solution X , and one subproblem node per $S \in \mathcal{S}_{k,\text{local}}$. We define two types of directed

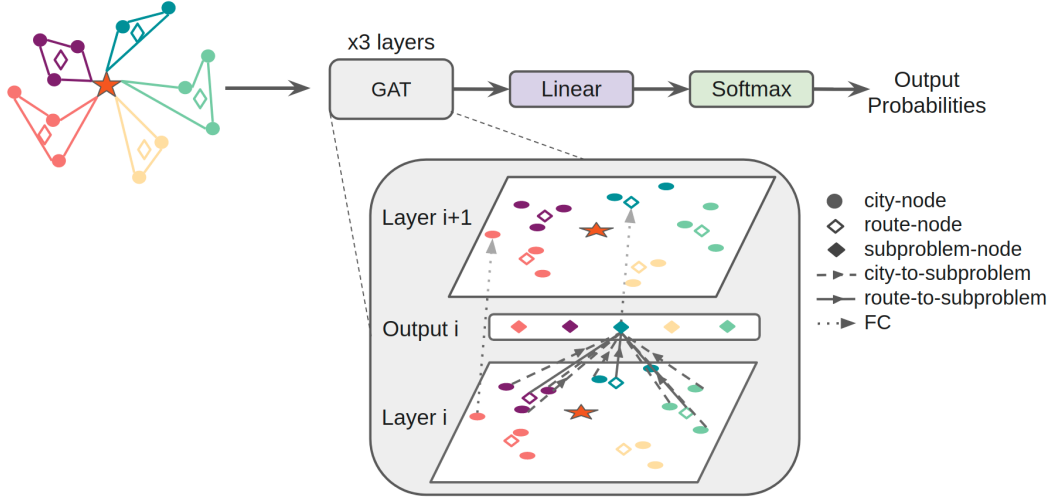


Figure 8: **Our Graph Attention Network (GAT) architecture.** At each step of our iterative framework (Figure 1(c)), we featurize the problem instance P with current solution X into city-node (filled circle) and route-node (empty diamond) features and city-to-subproblem and route-to-subproblem edges. The city-node input features at the i th graph attention layer is passed through a FC network to obtain the input city-node features at the $i + 1$ th graph attention layer. The subproblem-node (filled diamond) output features of the i th graph attention layer is passed through a FC network to obtain the input route-node features at the $i + 1$ th graph attention layer. The final graph attention layer’s subproblem-node output features are fed into a linear layers then a softmax to obtain the classification probabilities $p_\phi(S)$ for each subproblem.

edge connections: a *city-to-subproblem* edge connects a city-node to a subproblem-node if the city is in the subproblem and a *route-to-subproblem* edge connects a route-node to a subproblem-node if the route is in the subproblem. The input city-node features is fed into a fully connected (FC) network to obtain the input city-node features of the next graph attention layer, while the output subproblem-node features is fed into another FC network to obtain the input route-node features for the next graph attention layer, as each subproblem S corresponds to a single route r by construction as described in Subsection 4.1. The subproblem-node features of the final graph attention layer are fed into a linear layer followed by a softmax layer to obtain classification probabilities.

KL divergence loss. We minimize the KL divergence between the ground-truth soft labels $\ell(S)$ and the subproblem selector output probability distribution $p_\phi(S)$, where ϕ is the parameters of the subproblem selector

$$L(\phi; P) = D_{\text{KL}}(\ell \| p_\phi) = \sum_{S \in \mathcal{S}_{k, \text{local}}} \ell(S) \log \left(\frac{\ell(S)}{p_\phi(S)} \right). \quad (4)$$

One possible advantage of the KL divergence loss is that it places the most weight on the subproblems with high $\ell(S)$, which may help the neural network focus on a few subproblems with high immediate improvements rather than the many subproblems with low immediate improvement. In contrast, the Huber loss used in subproblem regression places equal emphasis on fitting subproblems with low and high immediate improvements.

A.2 Experiment Setup

We discuss the full experimental setup for training and evaluating the regression-based (Transformer) subproblem selector on the uniform CVRP distribution in this section while reserving any minor modifications for the clustered CVRP distributions, real-world CVRP distribution, VRP variants, and ablation studies for Appendix A.3, A.4, A.5, and A.6, respectively.

Uniform CVRP distribution. We generate CVRP instances of size $N = 500, 1000, 2000$ and 3000 following the same distribution of cities locations and demands as previous works [27, 18, 25, 19]: the depot and cities’ (x, y) locations are sampled uniformly from $[0, 1]^2$, each city’s demand d is sampled uniformly from $\{1, 2, \dots, 9\}$, and each vehicle has capacity $C = 50$. For each N , we sample $n_{\text{train}} = 2000$, $n_{\text{val}} = 40$, and $n_{\text{test}} = 40$ problem instances for the training, validation, and test set from the problem distribution.

Table 3: Uniform CVRP parameters.

Choices of N	$\{500, 1000, 2000, 3000\}$
Dist. of depot location	$\mathcal{U}([0, 1]^2)$
Dist. of city location	$\mathcal{U}([0, 1]^2)$
Dist. of city demand	$\mathcal{U}(\{1, \dots, 9\})$
Vehicle capacity	50

Table 4: Data splits.

Training	2000 instances
Validation	40 instances
Test	40 instances

Initialization solution. Our iterative learning to delegate framework (Figure 1) requires a rough initial solution X_0 . To generate X_0 for each problem instance, we employ a fixed initialization scheme in which the space is partitioned into 10 equally-sized angular sectors radiating outward from the depot. We then run the LKH-3 subsolver for a brief 100 steps on each region to produce initial routes. The initialization on average takes 6 seconds for $N = 500$, 18 seconds for $N = 1000$, 50 seconds for $N = 2000$, and 94 seconds for $N = 3000$ on a single CPU. Our initialization scheme is similar to the sweep-based algorithm proposed by Renaud and Boctor [29], which is a commonly used initialization scheme for iterative VRP solvers. Unless stated otherwise, we use the same initialization scheme in all methods to fairly compare each method’s ability to improve from a rough initialization.

Training data generation. We generate the training set by running our iterative framework and selecting subproblems as follows: for each instance P with initial solution X in the training set, we run the subsolver on each $S \in \mathcal{S}_{k, \text{local}}$ to compute the subsolution X_S and improvement $\delta(S)$. We update the solution from X to X' with $\arg \max_S \delta(S)$ then repeat the process on X' for a fixed number of steps $D_{\text{train}} = 30$ of our iterative framework. For the uniform CVRP distribution, we construct the $\mathcal{S}_{k, \text{local}}$ with $k = 10$ nearest routes to each route r in the current solution X . We compute the subsolution by running the LKH-3 subsolver for 500 steps, which takes around 6.7 seconds on a single CPU for a $k = 10$ subproblem composed of around 100 cities. We concatenate training data from multiple N ’s to train the subproblem regression model. As mentioned in the main text, most subproblems remain unchanged from X to X' , so we do not repeat duplicate subproblems in our generated training set; therefore, the number of unique subproblems in our training set may be around 3-8 times smaller than the total number of non-unique subproblems $n_{\text{train}} D_{\text{train}} \mathbb{E}[R] \approx n_{\text{train}} D_{\text{train}} \frac{N}{\mathbb{E}[d]}$ in the training set, where $\mathbb{E}[R]$ is the average number of routes in a solution.

As we find that the performance of the subproblem regression model trained on the concatenated $N = 500$ and 1000 data offers satisfactory performance, even when transferred to $N = 2000$ and 3000 , we do not collect training data for the latter two cases. Collecting training data is the most computationally intensive component of our work, and the computation time increases with larger N , larger k , and larger D_{train} . By restricting training data collection to $N = 500$ and 1000 , $k = 10$, and $D_{\text{train}} = 30$, the total time taken is around 10 hours on 200 CPUs.

Input features. To convert each subproblem S into the input to our Transformer-based subproblem regression model, we create a 3-dim input feature vector for each city consisting of the city’s (x, y) locations (centered around the depot’s (x, y) location) and the demand d (rescaled by the capacity).

Architecture and training hyperparameters. Our best Transformer-based model uses a model dimension $d_{\text{model}} = 128$, $n_{\text{heads}} = 8$ heads, $n_{\text{layers}} = 6$ layers, a feed-forward dimension of $d_{\text{ff}} = 512$,

Table 5: **Best architecture hyperparameters.**

Input dimension	3
Base model	Transformer
Model dimension d_{model}	128
Number of heads n_{heads}	8
Number of layers n_{layers}	6
Feed-forward dimension d_{ff}	512
Activation	ReLU
Layer Normalization	Yes
Dropout	0

Table 6: **Best training hyperparameters.**

Optimizer	Adam
Learning rate	0.001
Learning rate schedule	Cosine
Batch size	512
Number of gradient steps	40000
GPU	NVIDIA V100

ReLU activation, layer normalization, and no dropout. We train with Adam optimizer with a learning rate of 0.001, cosine learning rate decay, and a batch size of 2048 for 40000 gradient steps. All hyperparameters are selected on the validation set and frozen before evaluating on the test set for the final results.

Baseline learning methods. In Table 1, we compare our methods with two learning baselines: Attention Model (AM) [18] and NeuRewriter [6]. We use the pre-trained AM model provided by the author: <https://github.com/wouterkool/attention-learn-to-route>. The model is trained on problems of size 100 following the same distribution as ours. The model has two modes of prediction: greedy and sampling. We perform 1280 samples per instance, yet find the sampling performance worse than the greedy result. While the original paper reports better sampling performance than greedy when $N \leq 100$, we believe the exponentially larger solution space makes sampling good solutions difficult. We use a single NVIDIA V100 GPU with 20 CPUs to perform the evaluation.

For NeuRewriter, we retrain the network on problems of size 100 using the code provided by the author: <https://github.com/facebookresearch/neural-rewriter>, as no pre-trained model is available. Similarly to AM, we choose size 100 since it is the largest training problem size from the paper. We run into memory and fitting issue when trying to rerun their code on larger problem sizes, so we do not report the numbers here. We use a single NVIDIA V100 GPU with 20 CPUs to perform the evaluation.

A.3 Clustered and Mixed CVRP

Clustered CVRP distribution. We generate clustered CVRP distribution by modifying the distribution of city locations within the uniform CVRP distribution specified in Appendix A.2. Given the number of clusters n_c , we first generate n_c cluster centroids by sampling from $\mathcal{U}([0.2, 0.8]^2)$ as the (x, y) locations. Then, we generate the city nodes by first sampling a centroid uniformly at random, and then sampling the (x, y) location normally distributed with the mean at the centroid and standard deviation $\sigma = 0.07$. The (x, y) locations are clipped within the $[0, 1]^2$ box.

Mixed CVRP distribution. For the mixed distributions, we sample half of the city nodes according to the uniform distribution, and the other half according to a clustered distribution with n_c centers. This is the common practice used in standard CVRP benchmark datasets [39]. Note that we generate our new dataset instead of using the benchmark datasets because the CVRP benchmark datasets include mostly small scale $N \leq 500$ instances and has very few instances with $N \geq 100$.

Dataset composition. As we experiment over all combinations of $N \in \{500, 1000, 2000\}$, $n_c \in \{3, 5, 7\}$, and $\{\text{Clustered, Mixed}\}$, we generate smaller training, validation, and test set sizes with 500, 10, and 10 instances respectively for each combination. We visualize one clustered and one mixed instance in Figure 3.

Training and evaluation. Like in uniform CVRP, we do not collect the training set for the $N = 2000$ instances and concatenate the training set for all remaining combinations to create a single training set of $2 * 3 * 2 * 500 = 6000$ problem instances. We use identical architecture and training hyperparameters as listed in Appendix A.2, as we find that these hyperparameters perform reasonably well. We report test results on the test set of 10 instances for each of the $3 * 3 * 2 = 18$ settings separately.

Additional results. Here we include the full evaluation results on the test set for all clustered and mixed distributions. Figure 9 contains results for $N = 500$, Figure 10 contains results for $N = 1000$, and Figure 11 contains results for $N = 2000$. As mentioned in the above paragraph, all results are from a single trained model, which demonstrates superior speedup and improvement (when run for a reasonable time period) over the Random baseline. The results look similar to our previously reported results in other VRP distributions.

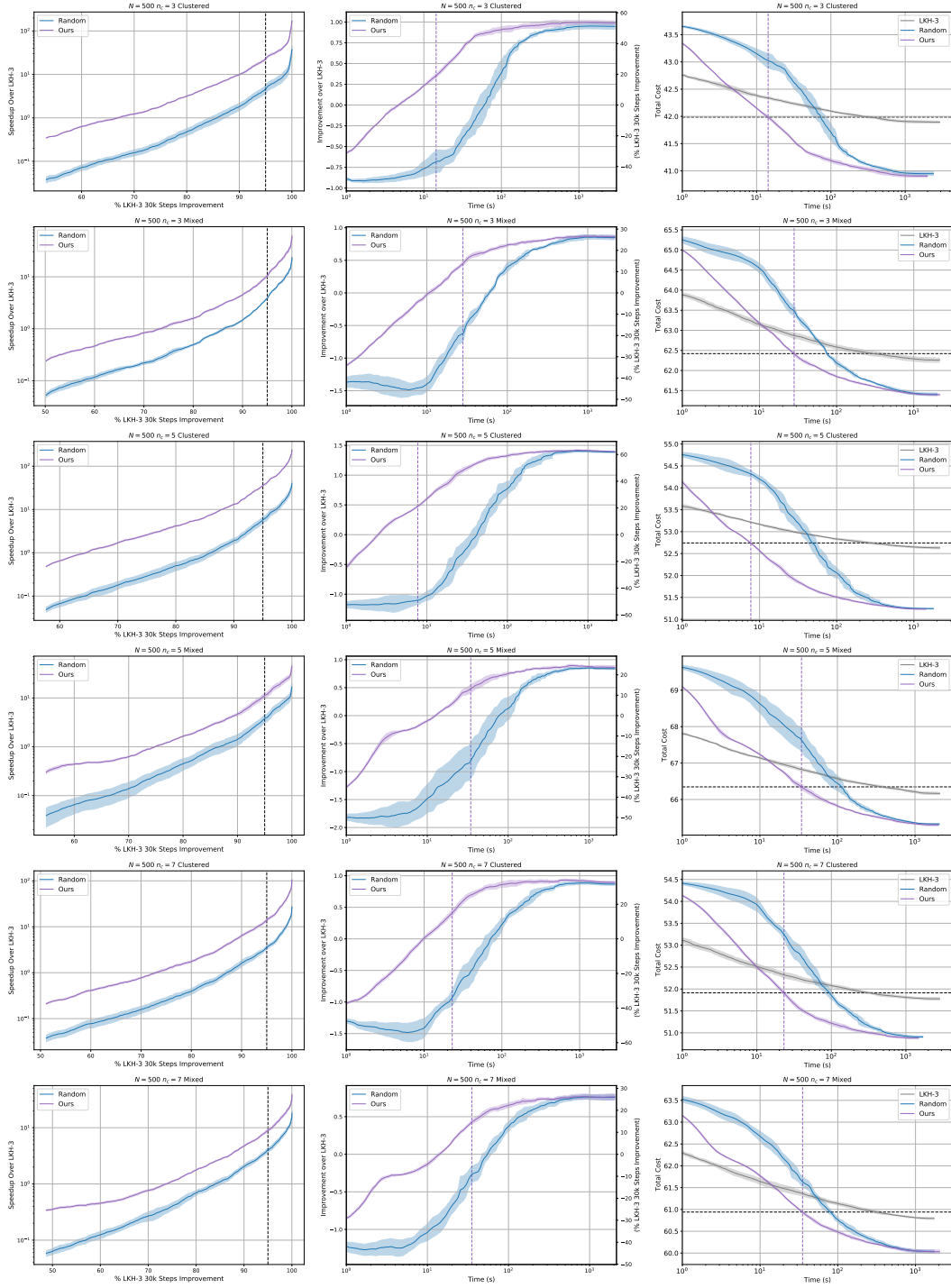


Figure 9: **Clustered and mixed CVRP distributions, $N = 500$.** Graphs of speedup (left column, higher is better), improvement (middle column, higher is better), and total cost (right column, lower is better). The right vertical axis in each improvement graph (middle column) indicates the improvement over LKH-3 as a percentage of the best improvement that LKH-3 attains over 30k steps. The vertical dashed black lines in the speedup graphs (left column) and the horizontal dashed black lines in the total cost graphs (right column) indicate solution qualities equal to 95% of the best LKH-3 solution qualities. The vertical dotted lines in the improvement graphs (middle column) and the total cost graphs (right column) indicate computation times required for our method to reach the aforementioned solution qualities.

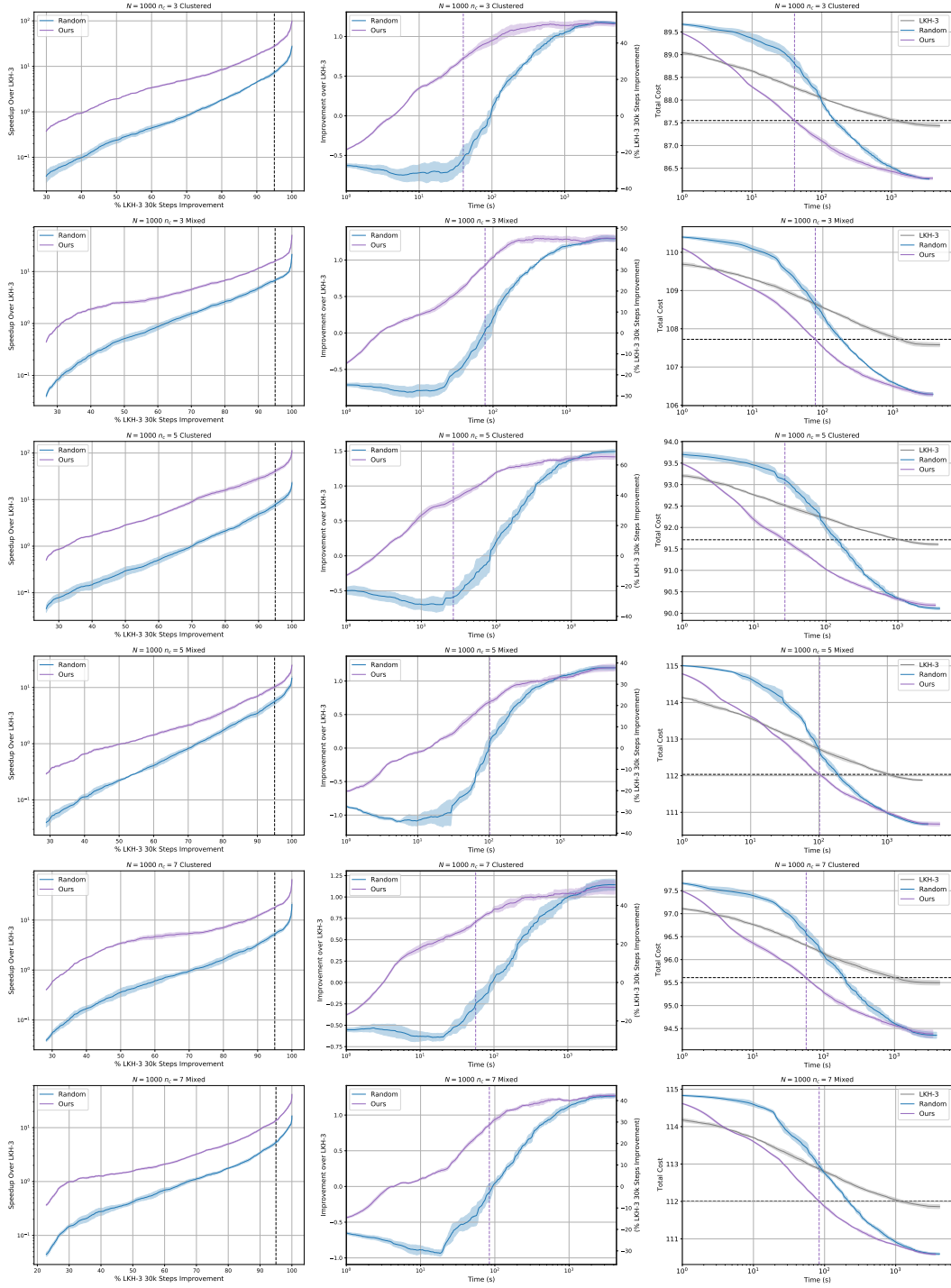


Figure 10: **Clustered and mixed CVRP distributions, $N = 1000$.** Graphs of speedup (left column, higher is better), improvement (middle column, higher is better), and total cost (right column, lower is better). The right vertical axis in each improvement graph (middle column) indicates the improvement over LKH-3 as a percentage of the best improvement that LKH-3 attains over 30k steps. The vertical dashed black lines in the speedup graphs (left column) and the horizontal dashed black lines in the total cost graphs (right column) indicate solution qualities equal to 95% of the best LKH-3 solution qualities. The vertical dotted lines in the improvement graphs (middle column) and the total cost graphs (right column) indicate computation times required for our method to reach the aforementioned solution qualities.

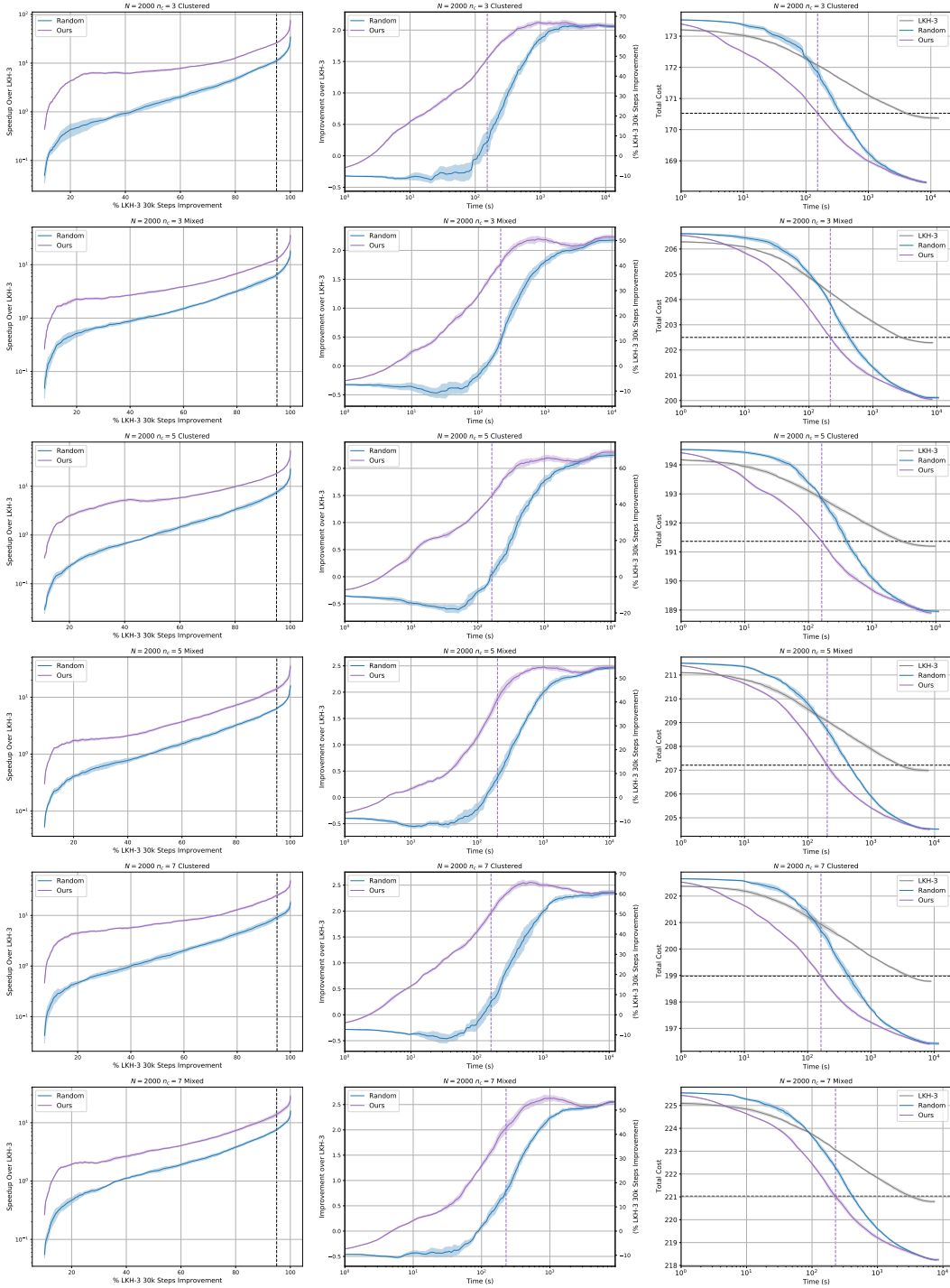


Figure 11: **Clustered and mixed CVRP distributions, $N = 2000$.** Graphs of speedup (left column, higher is better), improvement (middle column, higher is better), and total cost (right column, lower is better). The right vertical axis in each improvement graph (middle column) indicates the improvement over LKH-3 as a percentage of the best improvement that LKH-3 attains over 30k steps. The vertical dashed black lines in the speedup graphs (left column) and the horizontal dashed black lines in the total cost graphs (right column) indicate solution qualities equal to 95% of the best LKH-3 solution qualities. The vertical dotted lines in the improvement graphs (middle column) and the total cost graphs (right column) indicate computation times required for our method to reach the aforementioned solution qualities.

A.4 Out-of-distribution CVRPs

Here we describe the CVRP distributions and full results to demonstrate out-of-distribution generalization performance of our trained uniform CVRP and clustered CVRP models, with full training specifications in Appendix A.2 and Appendix A.3 respectively.

A.4.1 Uniform CVRP with $N = 3000$

We do not describe the setup here as it was previously described with the uniform CVRP distribution in Appendix A.2. In Figure 12, we see that the model trained on the clustered CVRP demonstrates slightly better improvement than the model trained on the uniform CVRP; otherwise the model performances are similar.

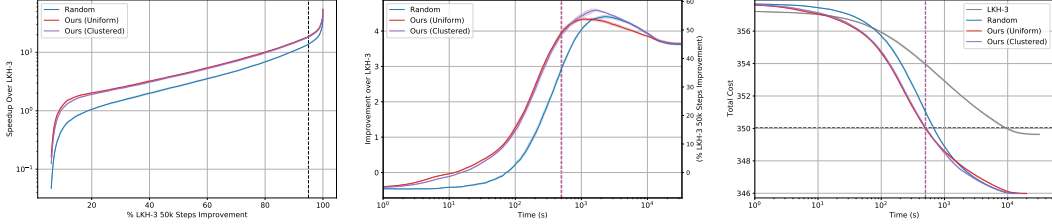


Figure 12: **Uniform CVRP distributions, $N = 3000$.** Graphs of speedup (left, higher is better), improvement (middle, higher is better), and total cost (right, lower is better). The left graph is the same as the left graph in Figure 6. The right vertical axis in the improvement graph (middle) indicates the improvement over LKH-3 as a percentage of the best improvement that LKH-3 attains over 30k steps. The vertical dashed black lines in the speedup graph (left) and the horizontal dashed black lines in the total cost graph (right) indicate a solution quality equal to 95% of the best LKH-3 solution quality. The vertical dotted lines in the improvement graph (middle) and the total cost graph (right) indicate computation times required for the our corresponding methods to reach the aforementioned solution quality.

A.4.2 Real-world CVRP

Excitingly, we see robust generalization performance of our previously trained models to problem instances from an unseen real-world CVRP distribution derived from the large-scale real-world CVRP dataset generated by Arnold et al. [4], which is open source at <https://antor.uantwerpen.be/xxlrouting/>.

Table 7: **Instance sizes N of original real-world instances from Arnold et al. [4].** Instances are subsampled without replacement to $N = 2000$ before feeding into our model.

Region	Centralized Depot	Eccentric Depot
Leuven	3000	4000
Antwerp	6000	7000
Ghent	10000	11000
Brussels	15000	16000
Flanders	20000	30000

Original real-world CVRP distribution. The original dataset contains 10 instances representing 5 different Belgium regions: Leuven, Antwerp, Ghent, Brussels, and Flanders. For each region, two instances are provided: one with a depot located at the center of all cities and the other with an eccentric depot located in the outskirts of the regions. We list the original sizes of each instance in Table 7 and visualize them in Figure 13.

This dataset focuses on long-haul deliveries, with the average solution route length ranging from 14.8 to 117.2. The authors randomly sample demand for each node from $\{1, 2, 3\}$ with probabilities 0.5, 0.3, and 0.2 respectively, and the capacity of the vehicle ranges from 20 to 50 for central depot and ranges from 100 to 200 for eccentric depot.

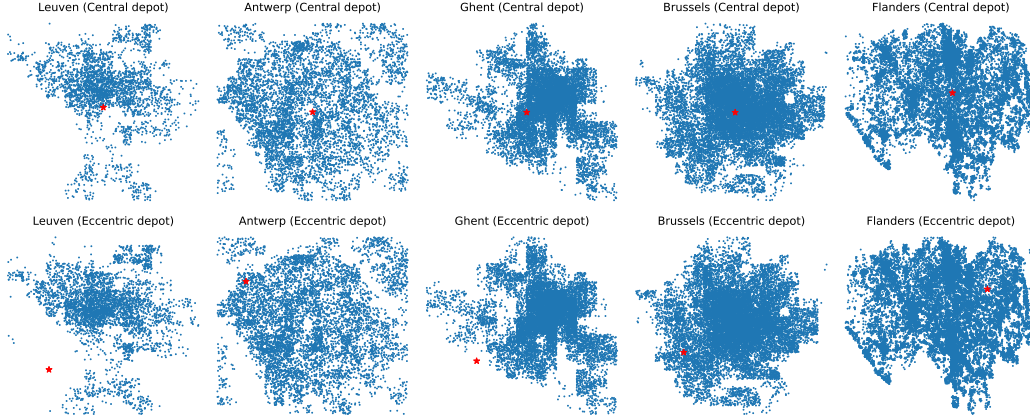


Figure 13: **Original real-world CVRP instances.** Five instances (top row) have centralized depots and five (bottom row) have eccentric depots.

Our real-world CVRP dataset. To apply our pre-trained models, we first convert the original real-world CVRP to be reasonably close to our training distributions. To generate each instance in our real-world CVRP distribution from an instance in the original dataset, we subsample the original instance to $N = 2000$ without replacement, resample each demand from our demand distribution $\mathcal{U}(\{1, 2, \dots, 9\})$, then set the vehicle capacity to $C = 50$. For each original instance, we generate 5 instances from our real-world CVRP distribution. Therefore, our validation and test sets contain 50 instances in total. One instance from our test set is visualized in Figure 3.

Additional results. We show the full transfer performance of the models trained on uniform and clustered CVRP to our real-world CVRP distribution in Figure 14. We see that the model trained on the clustered CVRP distributions significantly outperforms both the model trained on the uniform CVRP distribution and the Random baseline, whereas the model trained on the uniform CVRP distribution sometimes performs worse than the Random baseline. Encouragingly, the clustered model shows strong generalization performance in CVRP distributions which may be of practical value in the real world.

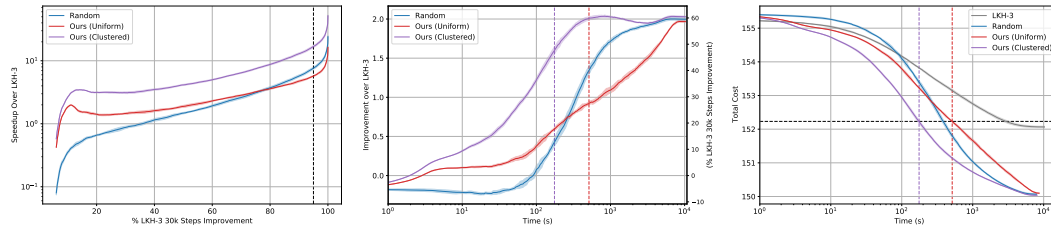


Figure 14: **Our real-world CVRP distribution.** Graphs of speedup (left, higher is better), improvement (middle, higher is better), and total cost (right, lower is better). The right vertical axis in the improvement graph (middle) indicates the improvement over LKH-3 as a percentage of the best improvement that LKH-3 attains over 30k steps. The vertical dashed black lines in the speedup graph (left) and the horizontal dashed black lines in the total cost graph (right) indicate a solution quality equal to 95% of the best LKH-3 solution quality. The vertical dotted lines in the improvement graph (middle) and the total cost graph (right) indicate computation times required for our corresponding methods to reach the aforementioned solution quality.

A.5 VRP Variants

Here we provide the full definition, experimental setup, and results for VRP variants discussed in Section 6.5: CVRPTW and VRPMPD.

A.5.1 CVRPTW (Capacitated Vehicle Routing Problem with Time Windows)

Problem formulation. We use the standard CVRPTW formulation found in Gehring and Homberger [10] and Solomon [33]. In addition to all the constraints in CVRP, each city node i has a time window $[e_i, l_i]$ where e_i is the earliest time to visit city i and l_i is the latest time to visit city i . Each city node i also has a service time s_i . The depot has a time window $[e_0, l_0]$ but no service time. Each vehicle departs the depot at time e_0 and follows a route r to satisfy the additional time window constraint. Let i and j be consecutive cities on route r , and let b_i^r denote the arrival time at city i of the vehicle serving route r . Then the arrival time at the next city j is $b_j = \max\{e_j, b_i + s_i + t_{ij}\}$ where t_{ij} is the travel time that equals the Euclidean distance from i to j . This specifies that if a vehicle arrives too early at j , then it needs to wait until the start time e_j of j . Meanwhile, the route becomes infeasible if the vehicle arrives later than l_j at j . Finally, the depot’s time window requires the route to travel back to the depot before l_0 . The objective is the same as in CVRP, i.e. minimizing the total Euclidean edge costs of all the routes, which is the standard objective used in the literature [17, 15]. The time window constraint imposed by this variant is related to other combinatorial optimization problems such as job shop scheduling [5].

Problem distribution. We generate CVRPTW instances following a similar procedure as in Solomon [33]: we first generate CVRP instances following the same uniform location and demand distribution as described in Section A.2. For the time window constraint, we set the time window for the depot as $[e_0, l_0] = [0, 3]$, and the service time at each i to be $s_i = 0.2$. We further set the time window for city node i by (1) sampling the time window center $c_i \sim \mathcal{U}([e_0 + t_{0,i}, l_0 - t_{i,0} - s_i])$, where $t_{0,i} = t_{i,0}$ is the travel time, equaling the Euclidean distance, from the depot to node i ; (2) sampling the time window half-width h_i uniformly at random from $[s_i/2, l_0/3] = [0.1, 1]$; (3) setting the time window for i as $[\max(e_0, c_i - h_i), \min(l_0, c_i + h_i)]$.

Training data generation. Unlike for CVRP distributions, we generate training data using $k = 5$ routes per subproblem instead of $k = 10$; doing so does not change the number of subproblems at each step, but helps speed up the generation process for two reasons: 1) running the subsolver on each subproblem takes around 3.4 seconds instead of 6.7 seconds for $k = 10$ and 2) updating current X with the subsolution X_S for a smaller subproblem S means that there will be more repeated subproblems from X to X' as other subproblems are less likely to be affected. Therefore, we are able to generate training data for $N = 500, 1000$, and 2000 with 2000 instances per N in around 10 hours total on 200 CPUs. An ablation study on the effect of k in uniform CVRP is provided in Appendix A.6.

Additional results. We show the full CVRPTW results in Figure 17, which also includes a comparison between subproblem regression and subproblem classification. Interestingly, while our method offers significant speedup over baseline methods and offers significant improvement over LKH-3 (relative to LKH-3’s total improvement over 30k steps) when run for a reasonable amount of time, the improvement over the LKH-3 baseline diminishes when run for a very long time. Indeed, our method terminates at a slightly worse total cost than LKH-3 for $N = 500$ when run for a very long time. However, as we show in the ablation over subproblem size k in Appendix A.6.1, we see that using $k = 10$ tends to offer better eventual improvement in uniform CVRP, so the diminishing improvement effect may be partially attributed to the fact that we use $k = 5$ for the CVRPTW experiments.

A.5.2 VRPMPD (Vehicle Routing Problem with Mixed Pickup and Delivery)

Problem formulation. This VRP variant models the backhauling problem where the vehicles are both delivering items to cities from the depot and picking up items from cities to bring back to the depot. We use the standard VRPMPD formulation as in Salhi and Nagy [30], where each city i either has a pickup order with load p_i or delivery order with load d_i . Each vehicle with a capacity C starts by loading all delivery orders along the route. Each time the vehicle visits a delivery city i , the vehicle’s load decreases by d_i ; conversely, each time the vehicle visits a pickup city j , the vehicle’s

load increases by p_j . A valid route requires that the vehicle’s load is no greater than C at every point along the route. Therefore, this variant imposes a more complicated capacity constraint than CVRP as the order of city visitation affects the feasibility of a route.

Problem distribution. We generate VRPMPD instances following a similar procedure as in Salhi and Nagy [30]: we take the CVRP instances following the same uniform location and demand distribution as defined in Appendix A.2, and we randomly assign half the cities pickup orders with $p_i \sim \mathcal{U}(\{1, 2, \dots, 9\})$ and the other half delivery orders with $d_i \sim \mathcal{U}(\{1, 2, \dots, 9\})$. We set the vehicle’s capacity to be $C = 25$ instead of 50 (as done for other VRPs) because this variant allows each routes to visit roughly 2x more cities than CVRP or CVRPTW with the same capacity, as the vehicle gains empty space after visiting the cities with delivery orders and can serve cities with pickup orders afterward.

Training data generation. We use the same $k = 5$ data generation process as described in Appendix A.5.1, but for VRPMPD instead of CVRPTW.

Additional results. We show the full VRPMPD results in Figure 18, which also includes a comparison between subproblem regression and subproblem classification. Similar to the behavior in CVRPTW, while our method offers significant speedup over baseline methods and offers significant improvement over LKH-3 (relative to LKH-3’s total improvement over 30k steps) when run for a reasonable amount of time, the improvement over the LKH-3 baseline diminishes when run for a very long time. However, as we show in the ablation over subproblem size k in Appendix A.6.1, we see that using $k = 10$ tends to offer better eventual improvement in uniform CVRP, so the diminishing improvement effect may be partially attributed to the fact that we use $k = 5$ for the VRPMPD experiments.

A.6 Ablation Studies

A.6.1 Subproblem Size k and Asymptotic Behavior in Uniform CVRP

We explore the effect of the subproblem size k , which specifies the number of nearest neighbor routes used to create each subproblem, and show that the choice of k may affect the asymptotic behavior of our iterative framework. We compare results between $k = 5$ and $k = 10$, using the same $k = 5$ data generation process as described in Appendix A.5.1 for uniform CVRP (not CVRPTW).

Experimental results. As shown in Figure 15, our method and the Random baseline with $k = 5$ may offer additional speedup over their $k = 10$ counterparts. However, they tend to converge earlier to worse eventual solution qualities when run for a very long time, though still better than the eventual solution qualities of LKH-3. These results suggest that subproblem selection with both $k = 5$ and $k = 10$ could combine the superior speedup of $k = 5$ with the better eventual solution qualities of $k = 10$.

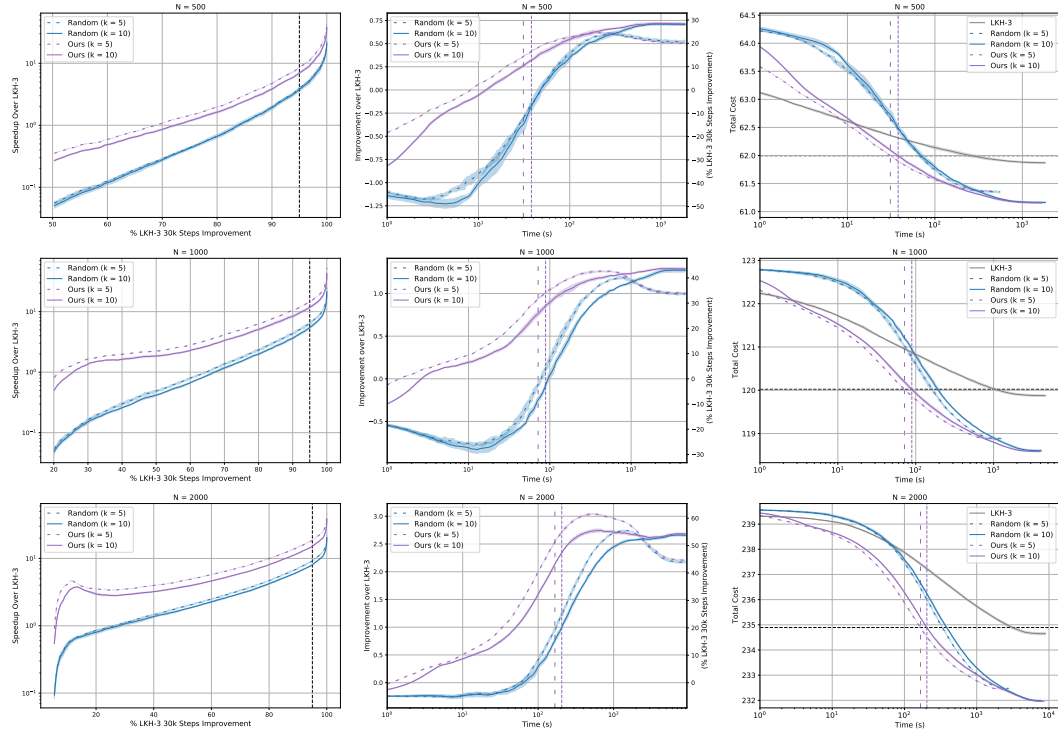


Figure 15: **Uniform CVRP distributions, comparing $k = 5$ and $k = 10$.** Graphs of speedup (left column, higher is better), improvement (middle column, higher is better), and total cost (right column, lower is better). The right vertical axis in each improvement graph (middle column) indicates the improvement over LKH-3 as a percentage of the best improvement that LKH-3 attains over 30k steps. We use loosely dotted lines to indicate $k = 5$. The vertical dashed black lines in the speedup graphs (left column) and the horizontal dashed black lines in the total cost graphs (right column) indicate solution qualities equal to 95% of the best LKH-3 solution qualities. The vertical dotted lines in the improvement graphs (middle column) and the total cost graph (right column) indicate computation times required for our methods to reach the aforementioned solution qualities.

A.6.2 Subproblem Regression vs Classification

Table 8 summarizes the key advantages of subproblem regression over subproblem classification: subproblem regression is much faster to train and only requires a single trained model over all problem instance sizes.

Table 8: **Training time of subproblem regression and subproblem classification.** Subproblem regression models are simultaneously trained over all problem sizes where subproblem classification models are trained on individual problem sizes. Training times are similar for subproblems with size $k = 5$ and $k = 10$, so we do not distinguish between the two cases in this table. Note that we do not use $N = 2000$ data for subproblems with size $k = 10$ for training, as explained in Appendix A.2, but we do use $N = 2000$ data for subproblems with size $k = 5$ for training, as explained in Appendix A.6.1.

N	Regression	Classification
500	6 hours total	6 hours
1000		12 hours
2000		24 hours

Here we provide experimental results comparing subproblem regression and classification, which are respectively introduced and compared in Section 5 and Appendix A.1.

Classification setup. While we previously describe the setup of the regression model in Appendix A.2, here we describe the additional modifications made in the classification setup compared with the regression setup.

1. While we do not need to collect separate training data from the regression setup, we need to process the label to be $\ell(S)$ as defined in Appendix A.1 rather than $\delta(S)$.
2. In addition to extracting 3-dim feature vector for each city in P , we also extract 8-dim feature vector for each route in the current solution X consisting of: the average, max, and min (x, y) locations of cities in the route (shifted by the depot's (x, y) location); the sum of demands of cities in the route; and the route's distance.
3. We find the best GAT architecture hyperparameters to be a model (hidden) dimension of 128, 1 attention head, and 3 graph attention layers.
4. As the classification network does not handle multiple problem sizes (e.g. $N = 500$ and $N = 2000$) naturally due to large differences in the number of subproblems, we train each classification model on data from a single problem instance size. However, this is not a fundamental limitation, and future works may explore training a subproblem classification network on multiple problem sizes.
5. We train our best classification models with batch sizes of 256, 256, and 512 *problem instances* respectively for $N = 500, 1000, 2000$. We emphasize that the batches here are batches of *problem instances*, where each problem instance graph inherently contains $|\mathcal{S}_{k,\text{local}}|$ subproblems as illustrated earlier in Figure 8, rather than batches of *subproblems* as in the regression setup.
6. Training takes around 6 hours for $N = 500$, 12 hours for $N = 1000$, and 24 hours for $N = 2000$ on a single NVIDIA V100 GPU.

Comparison on uniform CVRP. We compare the performance of subproblem regression and subproblem classification for $N = 500$ and 1000 uniform CVRP and $k = 10$. Despite requiring significantly less training time, we observe that subproblem regression does not suffer a loss in performance against the more specialized subproblem classification, as seen in Figure 16. Thus, we chose to focus on subproblem regression in this paper as it offers generalization over multiple problem sizes while enjoying significantly less training time.

Comparison on VRP variants. We compare the performance of subproblem regression and subproblem classification for $N = 500, 1000$ and 2000 CVRPTW and VRPMPD and $k = 5$. Interestingly, we see that subproblem classification somewhat outperforms subproblem regression in Figure 17 and Figure 18. Therefore, future works may benefit from trying both regression and classification and possibly adapting subproblem classification to train over multiple problem sizes.

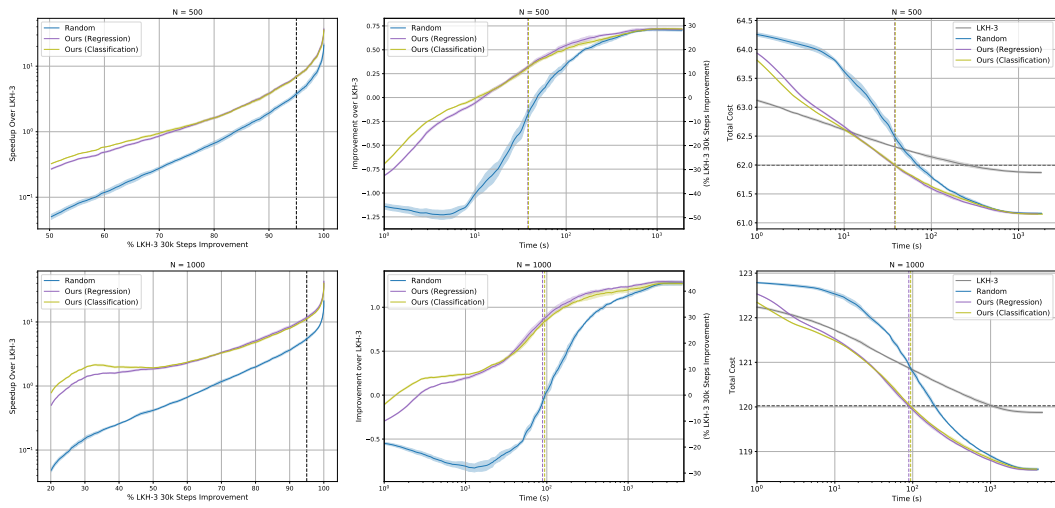


Figure 16: **Uniform CVRP distribution, regression vs classification.** Graphs of speedup (left column, higher is better), improvement (middle column, higher is better), and total cost (right column, lower is better). The vertical dashed black lines in the speedup graphs (left column) and the horizontal dashed black lines in the total cost graphs (right column) indicate solution qualities equal to 95% of the best LKH-3 solution qualities. The vertical dotted lines in the improvement graphs (middle column) and the total cost graph (right column) indicate computation times required for our methods to reach the aforementioned solution qualities.

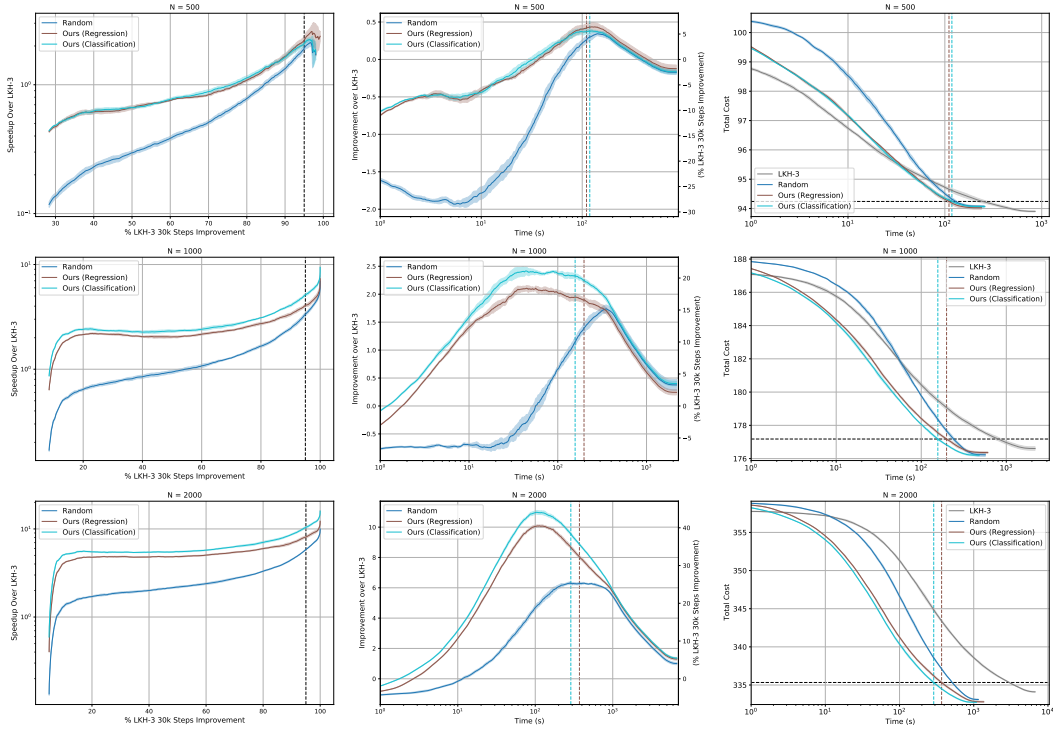


Figure 17: **Uniform CVRPTW distributions.** Graphs of speedup (left column, higher is better), improvement (middle column, higher is better), and total cost (right column, lower is better). The right vertical axis in each improvement graph (middle column) indicates the improvement over LKH-3 as a percentage of the best improvement that LKH-3 attains over 30k steps. The vertical dashed black lines in the speedup graphs (left column) and the horizontal dashed black lines in the total cost graphs (right column) indicate solution qualities equal to 95% of the best LKH-3 solution qualities. The vertical dotted lines in the improvement graphs (middle column) and the total cost graph (right column) indicate computation times required for our methods to reach the aforementioned solution qualities.

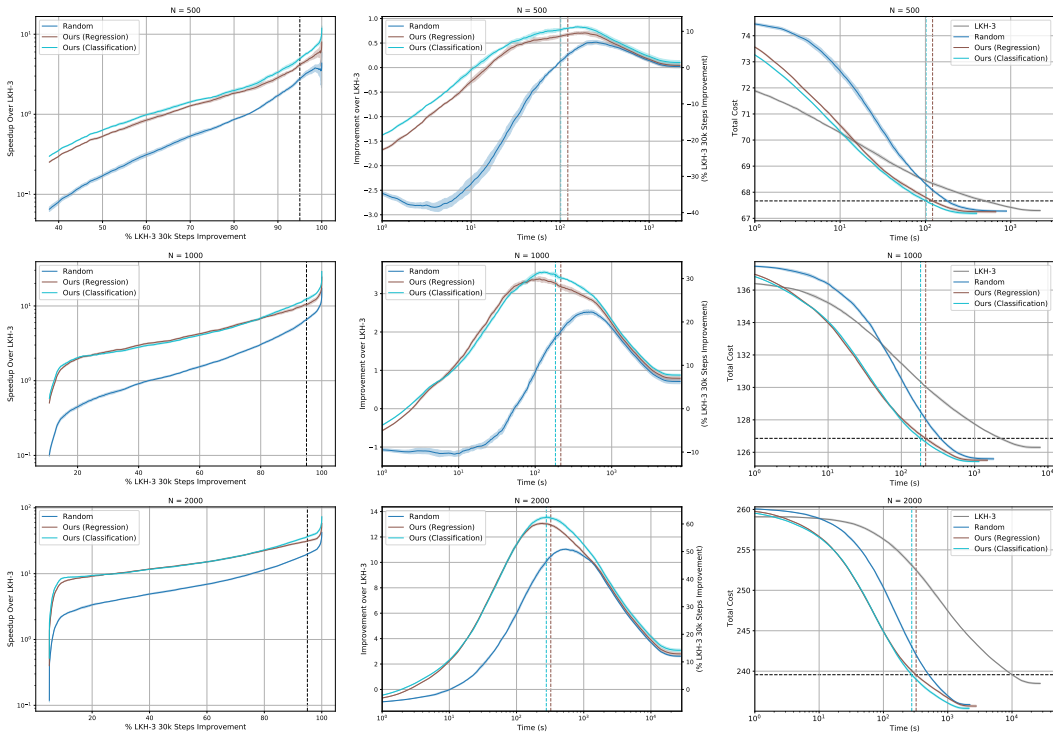


Figure 18: **Uniform VRPMPD distributions.** Graphs of speedup (left column, higher is better), improvement (middle column, higher is better), and total cost (right column, lower is better). The right vertical axis in each improvement graph (middle column) indicates the improvement over LKH-3 as a percentage of the best improvement that LKH-3 attains over 30k steps. The vertical dashed black lines in the speedup graphs (left column) and the horizontal dashed black lines in the total cost graphs (right column) indicate solution qualities equal to 95% of the best LKH-3 solution qualities. The vertical dotted lines in the improvement graphs (middle column) and the total cost graph (right column) indicate computation times required for our methods to reach the aforementioned solution qualities.